

## MICROSTRUCTURE AND OXIDATION RESISTANCE OF Pd+Zr AND Pd+Hf CO-DOPED ALUMINIDE COATINGS DEPOSITED ON MAR-M247 NICKEL SUPERALLOY

J. Romanowska \*, M. Zagula-Yavorska

Rzeszów University of Technology, Department of Materials Science, Faculty of Mechanical Engineering and Aeronautics, Rzeszów, Poland

(Received 05 December 2022; Accepted 07 August 2023)

### Abstract

*Pd+Zr and Pd+Hf co-doped aluminide coatings were deposited on the nickel superalloy Mar-M247 by palladium electroplating followed by zirconization-aluminization or hafnization-aluminization processes. Both coatings consisted of two zones, the outer and the interdiffusion zone consisting of the  $\beta$ -(Ni,Pd)Al phase. Hafnium and zirconium formed inclusions deposited at the edge of the zones and near the surface (only in the Zr+Pd modified coating). The oxidation resistance of the aluminide coating co-doped with Pd+Zr was significantly better than the one co-doped with Pd+Hf. The hafnium content in the Pd+Hf co-doped coating could exceed the limit.*

**Keywords:** Nickel superalloys; Aluminide coatings; Hafnium; Zirconium; Oxidation

### 1. Introduction

Thermal barrier coatings (TBCs) are applied to improve the efficiency of gas turbine engines. They can decrease the temperature on the turbine blades made of nickel based superalloys by more than 150K. Thanks to these coatings, gas turbine engines can operate at temperatures above the melting point of nickel-based superalloys [1]. Aluminide coatings are often used as bond coats due to their oxidation resistance, and small amounts of noble or reactive metals incorporated into the coating significantly improve its protective properties [2, 3]. Aluminum forms an oxide that protects the superalloy from oxidation. Platinum, which dissolves in the NiAl phase and forms a (Ni,Pt)Al phase, improves the oxide scale adhesion to the substrate, slows the oxide growth [4] and prevents diffusion of refractory elements from the substrate [5]. Unfortunately, the “rumpling” phenomenon reduces the cyclic thermal stresses resistance. The rumpling of the Pt-modified aluminide coating is caused by the thermal expansion mismatch between the aluminide and the underlying superalloy and plastic deformation of the coating and the oxide [6]. Palladium dissolving in NiAl to form (Ni,Pd)Al phase, improves the cyclic oxidation and hot corrosion resistance of the coating [7], accelerates  $\theta$ -Al<sub>2</sub>O<sub>3</sub> to  $\alpha$ -Al<sub>2</sub>O<sub>3</sub> transformation [8] and increases  $\beta$ -NiAl phase lifetime [9]. The addition of small amounts of reactive elements to aluminide coatings

with [10] or without [11] noble metals results in further improvement of the coatings’ oxidation behavior [12], oxide scale adhesion and growth rate reduction [13]. Reactive elements form oxides that precipitate at the oxide/coating interface [14]. According to the dynamic segregation theory these oxide pegs, [15], slow down Al outward diffusion and change the oxide scale growth mechanism to inward oxygen diffusion and reduce the oxide growth rate [16]. Hafnium diffusing from the substrate into the coating and aluminum oxide, improves the propensity for oxides rumpling [17] and high temperature mechanical properties [18]. Zirconium dioxide reduces the oxide creep rate [19], whereas a small addition of zirconium (0.1%at.) reduces cracking of the spalling scale [11].

The strategy of co-doping, i.e., introducing more than one dopant, leads to better improvement of thermal and mechanical properties of aluminide coatings than single doping [13, 16]. Zirconium implemented into the Pt-modified aluminide coating forms oxide pegs and increases the spallation resistance of the coating. Zirconium and platinum were deposited by the electroplating process. Subsequently, the aluminide coating was deposited in the gaseous phase aluminization process on a second-generation Ni-base single crystal superalloy [1]. Co-doped (Zr and Pt) aluminide coatings reduced the tendency of oxide scale spallation, lowered the oxidation rate constant and surface rumpling better

Corresponding author: jroman@prz.edu.pl

<https://doi.org/10.2298/JMMB221205021R>



than single-doped aluminide coatings [1]. Therefore, it seems, that the thermal and mechanical properties of other co-doped aluminide coatings are worth further attention.

This paper presents the results of investigation of Pd+Zr and Pd+Hf co-doped aluminide coatings deposited on Mar-M247 nickel-based superalloy. Mar-M247 is used for turbine blades, rotors and stators [20]. It is a polycrystalline cast nickel-based superalloy. It has a multiphase structure consisting of  $\gamma$  and  $\gamma'$  phases. Aluminium content of 5-6 at.% is sufficient to form  $Al_2O_3$  layer during oxidation, but this layer is neither thick nor continuous enough to protect the superalloy against oxidation. Therefore, protective coatings should be applied [21]. According to Mei et al. [21], the oxidation resistance of NiCoCrAlTaY coated Mar M247 superalloy is better than that of the uncoated one as far as the corrosion in dry air [21] or in molten  $Na_2SO_4$  vapour [22] are concerned. Qian et al. [23] proved that  $ZrO_2$  nanoparticles incorporated into PtAl coatings improved the oxide scale growth rate and rumpling resistance of the coating.

Although the oxidation resistance of coated and uncoated Mar-M247 was thoroughly investigated and many kinds of coatings were analyzed, the Pd+Zr and Pd+Hf co-doped aluminide coatings have not yet been applied and analyzed. Therefore, this paper deals with the analysis of chemical and phase composition of the Pd+Zr and Pd+Hf co-doped aluminide coatings and comparison of their oxidation resistance after 500 hours of oxidation in the air at 1100°C.

## 2. Experimental

The chemical composition of the Mar-M247 (polycrystalline) substrate is as follows: 0.15 wt-% C, 10 Co, 8.25 Cr, 5.5 Al, 10 W, 3 Ta, 0.7 Mo, 1 Ti, 0.5 Fe, 0.015B, 0.005 Zr, 1.5 Hf, balance Ni. The palladium layers were deposited electrochemically on circular samples, with a diameter of 14 mm and a height of 4 mm. This 3-step procedure was described in details in references 24 and 25. The parameters of the Pd plating process were as follows: current density - 10 mAcm<sup>-2</sup>, bath temperature - 550C, time - 11 min, palladium chloride concentration- 13.3 g dm<sup>-3</sup>. Then, aluminide coatings were deposited on the samples with palladium layers in a zirconizing-aluminizing process, described in details in reference 26 or hafnizing-aluminizing process, described in details in reference 27. These processes consisted of four stages: a) heating to 1040°C, b) aluminizing for 6 hours at 1040°C, c) zirconizing with aluminizing or hafnizing with aluminizing for 6 hours at 1040°C, d) cooling to room temperature. The samples were oxidized at 1100°C for 20 hours, then cooled slowly to the room temperature, weighted and inspected.

Twenty five cycles were executed. Surface and cross-section of coated samples before and after oxidation were analyzed by microscopic methods (SEM, EDS) and XRD analysis with Cu anode. The Powder Diffraction File, International Centre for Diffraction Data, Pennsylvania, USA 2002, database was used.

## 3. Results

### 3.1. Microstructure of the Pd+ Zr co-doped coating before oxidation

Figure 1 presents the surface morphology and EDS spectrum of the coating before oxidation. The coating consisted mainly of Ni, Al, some Pd and a small amount of refractory elements (Co, Cr, Fe) diffused from the substrate (Fig.1a, Table 1). The chemical composition corresponded to the  $\beta$ -NiAl phase. Zirconium was located in small precipitates (Fig. 1b, Table 2). The XRD pattern (Fig.2) confirmed the presence of the  $\beta$ -NiAl phase, whose lattice parameter increased (0.6%). This proves that the

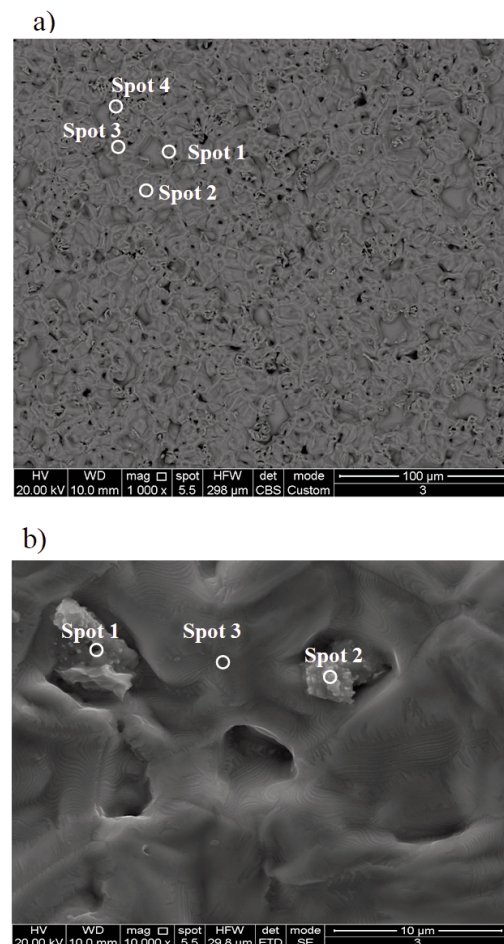


Figure 1. Surface morphology (a) and zirconium-rich particles distribution (b) in the Pd+Zr co-doped aluminide coating deposited on the Mar-M247 substrate



palladium dissolved in the  $\beta$ -NiAl phase, enlarged the  $\beta$ -NiAl crystal lattice parameter and the  $\beta$ -(Ni,Pd)Al phase was formed. Moreover, the existence of Hf rich phases (HfH<sub>1.628</sub> [28, 29] with the 0.02% smaller lattice parameter or HfC [2, 15] with the 0.6% larger lattice parameter) was revealed.

**Table 1.** Chemical composition on the surface of the Pd+Zr co-doped aluminide coating deposited on the Mar-M247 substrate (at.%), Fig.1a

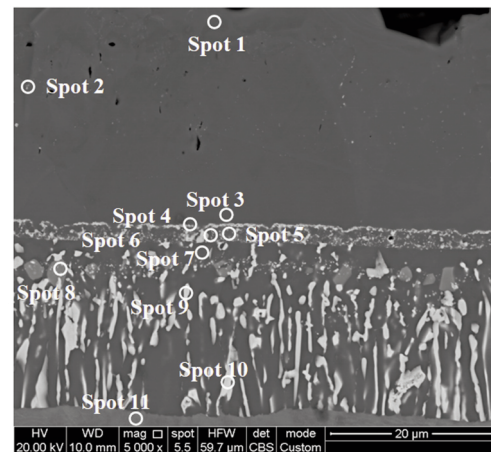
| Spot | Al   | Pd  | Cr  | Fe  | Co  | Ni   |
|------|------|-----|-----|-----|-----|------|
| 1    | 44.9 | 4.1 | 0.8 | 0.7 | 4.8 | 44.7 |
| 2    | 29.3 | 4.9 | 1.0 | 1.4 | 5.5 | 58.0 |
| 3    | 44.5 | 5.3 | 0.6 | 0.8 | 4.0 | 44.8 |
| 4    | 15.0 | 3.8 | 0.8 | 1.5 | 6.6 | 72.4 |

**Table 2.** Chemical composition on the surface of Pd+Zr aluminide coating deposited on the Mar-M247 substrate (at.%), Fig.1b

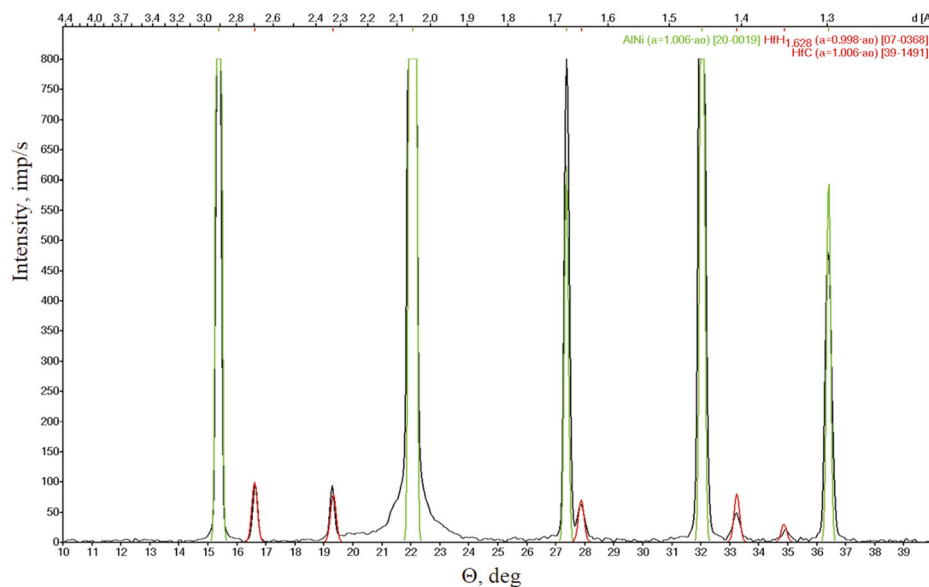
| Spot | Al   | Zr  | Pd  | Cr  | Fe  | Co  | Ni   |
|------|------|-----|-----|-----|-----|-----|------|
| 1    | 54   | 1.2 | 5.7 | 0.2 | 0.6 | 2.8 | 35   |
| 2    | 54.9 | 1.1 | 5.4 | 0.6 | 0.6 | 2.6 | 35.1 |
| 3    | 39.9 | 0   | 5.8 | 0.3 | 0.7 | 4.0 | 49.3 |

Figure 3 presents the cross-section of the coating. It consisted of two zones, the outer one, 25  $\mu$ m thick and the interdiffusion one, 20  $\mu$ m thick. The outer zone consisted of the  $\beta$ -(Ni,Pd)Al phase, as confirmed by the XRD analysis (Fig.2). SEM-EDS analysis of the chemical composition revealed small amounts of zirconium (0.6 at.%), hafnium (1.9 at.%) and refractory elements (Cr, Co, Ta, W). The aluminum content decreased from 49.4 at.% close to the surface (Fig.3, spot 1) to 36.6 at.% close to the boundary

between the outer and interdiffusion zones (Fig.3, Table 3, spot 3). The palladium content decreased from 5.3 at.% to 3 at.%, whereas the nickel content increased from 40.5 to 47.5 at.% (Fig. 3, Table 3, spot 1 and 3, respectively). Such a distribution is typical for diffusive aluminide coatings [30]. Hafnium and zirconium rich inclusions were observed on the border of two zones (Fig.3, spot 4). The interdiffusion zone contained a large number of precipitates of refractory elements that diffused from the substrate (Fig.3 spots 5-10). The phenomenon of two zones, a chain of hafnium and zirconium rich precipitates on the border of the zones and inclusions containing refractory elements in the interdiffusion zone on the MAR M200+Hf superalloy was reported by Pytel et al. [30].



**Figure 3.** The cross-sectional microstructure of the Pd+Zr co-doped aluminide coating deposited on the Mar-M247 substrate



**Figure 2.** XRD diffraction of the Pd+Zr co-doped aluminide coating deposited on the Mar-M247 substrate



**Table 3.** Chemical composition on the cross-section of the Pd+Zr co-doped aluminide coating deposited on the Mar-M247 substrate (at.%), Fig.3

| Spot | Al   | Zr  | Mo  | Pd  | Ti   | Cr   | Fe  | Co   | Ni   | Hf   | Ta   | W    |
|------|------|-----|-----|-----|------|------|-----|------|------|------|------|------|
| 1    | 49.4 | -   | -   | 5.3 | -    | 0.5  | 0.6 | 3.7  | 40.5 | -    | -    | -    |
| 2    | 31.3 | 0.6 | -   | 3.8 | 4.6  | 3.5  | 0.6 | 5.9  | 41.7 | 1.9  | 5.4  | 0.9  |
| 3    | 36.6 | -   | -   | 3.0 | 0.8  | 4.5  | 0.5 | 6.7  | 47.5 | -    | -    | -    |
| 4    | 25.1 | 2.4 | -   | 2.8 | 9.8  | 4.9  | 0.4 | 5.4  | 35.3 | 9.4  | 3.9  | 0.6  |
| 5    | 11.7 | 0.6 | 4.5 | 1.6 | 1.4  | 35.0 | 0.5 | 3.6  | 20.2 | 0.8  | -    | 20.1 |
| 6    | 32.1 | -   | -   | 2.4 | 2.1  | 8.3  | 0.4 | 7.6  | 43.8 | 2.1  | 0.8  | 0.3  |
| 7    | 34.8 | -   | -   | 2.5 | 1.0  | 5.1  | 0.5 | 7.0  | 47.8 | 0.6  | -    | 0.5  |
| 8    | 3.9  | -   | 0.7 | 0.3 | 0.5  | 72.2 | 0.7 | 4.4  | 10.1 | -    | 0.5  | 6.8  |
| 9    | 7.3  | -   | 2.4 | 0.7 | 0.5  | 24.5 | 1   | 17.8 | 21.3 | -    | 1.0  | 23.4 |
| 10   | 5.0  | -   | -   | -   | 13.4 | 4.3  | -   | 4.1  | 16   | 28.7 | 28.5 | -    |
| 11   | 15.6 | -   | 0.1 | 0.1 | 1.7  | 8.8  | 0.3 | 9.2  | 60.2 | 1.1  | 0.7  | 2.0  |

### 3.2. Microstructure of the Pd+ Zr co-doped coating after oxidation

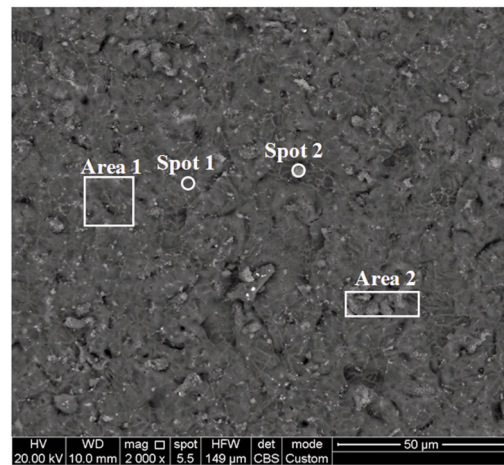
The oxidized coating consisted mainly of oxygen and aluminum with small amounts of tungsten, titanium, chromium, iron, cobalt nickel, hafnium, and zirconium (Fig.4, Table 4). After 500 hours of oxidation scale remained almost intact, only small spalled areas were visible. The scale was composed of  $\alpha$ -Al<sub>2</sub>O<sub>3</sub>, ZrO<sub>2</sub>, HfO<sub>2</sub>, AlNi<sub>3</sub>, TiO<sub>2</sub> and Ni<sub>81</sub>Pd<sub>19</sub> (Fig.5). The lattice parameter of  $\alpha$ -Al<sub>2</sub>O<sub>3</sub> phase was 0.2 % enlarged, whereas the lattice parameter of the AlNi<sub>3</sub> phase was 0.7% enlarged. That suggest, that palladium dissolved in these lattices and enlarged them [28, 29].

The scale was 6  $\mu$ m thick, composed of Al<sub>2</sub>O<sub>3</sub> with some cracks up to 10  $\mu$ m deep (Fig.6). The structure of the coating below the scale remained intact. Two zones were clearly visible: the outer and the interdiffusion zone, both 20  $\mu$ m thick. The outer zone contained mainly nickel, aluminum and small amounts of palladium and other refractory elements. The interdiffusion zone contained mainly nickel and aluminum with a large number of precipitates of refractory elements. These two zones were separated by a chain of zirconium and hafnium rich inclusions. (Fig. 6, spots 5,6) During oxidation the aluminum concentration in the outer layer significantly decreased (from more than 40 at. %, Table 3, to less than 20 at. Table 5). This fact can be attributed to

Al<sub>2</sub>O<sub>3</sub> formation. Moreover, hafnium and zirconium diffused to the surface (Table 5, spot 1) and formed ZrO<sub>2</sub> and HfO<sub>2</sub> (Fig. 6, Table 5).

### 3.3. Microstructure of the Pd+Hf co-doped coating before oxidation

Figure 7 presents the surface morphology and EDS spectrum of the coating before oxidation. The coating consisted mainly of Ni, Al, some Pd and small amounts of refractory elements (Co, Cr, Fe) that

**Figure 4.** Surface morphology of the oxidized Pd+Zr co-doped aluminide coating deposited on the Mar-M247 substrate**Table 4.** Chemical composition on the surface of oxidized Pd+Zr co-doped aluminide coating deposited on the Mar-M247 substrate (at.%), Fig.4

| Area/Spot | O    | Al   | W   | Zr  | Ti  | Cr  | Fe  | Co  | Ni  | Hf  |
|-----------|------|------|-----|-----|-----|-----|-----|-----|-----|-----|
| Area 1    | 56.2 | 42.4 | -   | 0.6 | 0.1 | 0.1 | -   | 0.1 | 0.4 | 0.1 |
| Area 2    | 55.0 | 43.0 | 0.1 | 0.7 | 0.2 | 0.1 | 0.1 | 0.1 | 0.6 | 0.1 |
| Spot 1    | 57.5 | 41.4 | -   | -   | 0.1 | 0.2 | -   | 0.1 | 0.6 | 0   |
| Spot 2    | 57.2 | 39   | -   | 0.8 | 0.1 | 0.2 | 0.1 | 0.2 | 2.0 | 0.1 |

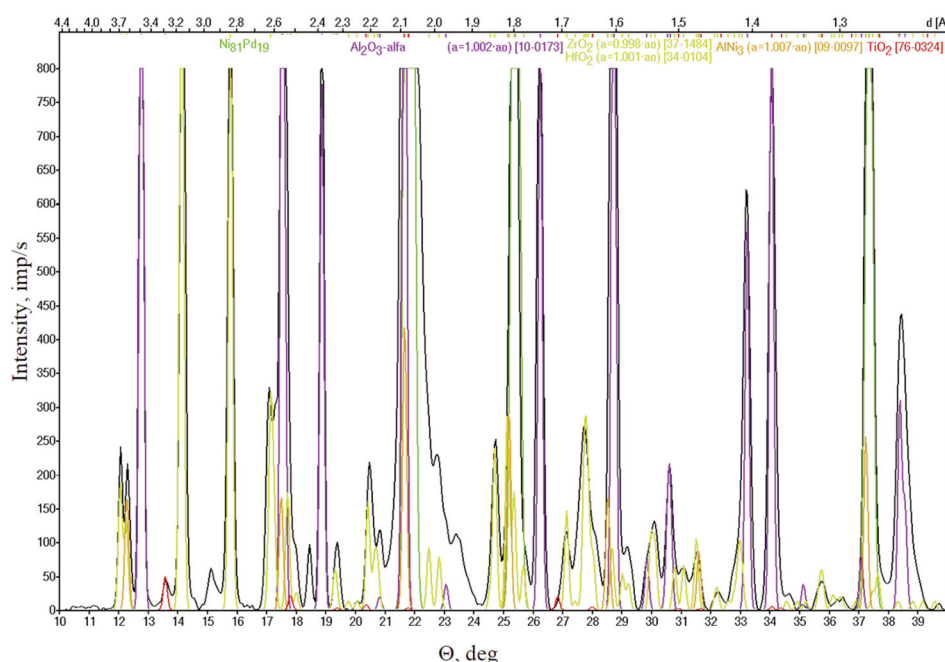


Figure 5. XRD diffraction of oxidized Pd+Zr co-doped aluminide coating deposited on the Mar-M247 substrate

Table 5. Chemical composition on the cross-section of the oxidized Pd+Zr co-doped aluminide coating deposited on the Mar-M247 substrate (at.%), Fig.6

| Spot | O    | Al   | Zr  | Mo  | Pd  | Ti   | Cr   | Fe  | Co   | Ni   | Hf   | Ta  | W    |
|------|------|------|-----|-----|-----|------|------|-----|------|------|------|-----|------|
| 1    | 61.2 | 19.5 | 2.5 | -   | 0.5 | -    | 0.4  | -   | -    | 3.8  | 12   | -   | -    |
| 2    | -    | 19.9 | -   | -   | 1.7 | 1.2  | 4.9  | 0.4 | 7.4  | 61.7 | -    | 1.2 | 1.6  |
| 3    | -    | 19.5 | -   | 0.1 | 1.6 | 1.3  | 4.9  | 0.3 | 7.6  | 61.8 | -    | 1.2 | 1.7  |
| 4    | -    | 17.7 | -   | -   | 1.3 | 11.8 | 4.6  | 0.3 | 6.4  | 52.2 | 1.4  | 2.7 | 1.4  |
| 5    | -    | 14.3 | 2.1 | -   | 1.7 | 1.4  | 4.6  | 0.3 | 6.2  | 51.7 | 15.7 | 0.8 | 3.1  |
| 6    | -    | 19.5 | 0.1 | 0.1 | 1.5 | 1.6  | 4.8  | 0.4 | 7.5  | 60.8 | 0.9  | 0.9 | 1.8  |
| 7    | -    | 19.4 | -   | 0.1 | 1.5 | 1.2  | 4.8  | 0.4 | 7.5  | 62.2 | -    | 1.2 | 1.8  |
| 8    | -    | 3.0  | -   | 2.8 | -   | 0.8  | 21.7 | 0.6 | 12.4 | 25.3 | -    | 2.6 | 30.8 |
| 9    | -    | 11.8 | -   | 0.2 | 0.6 | 0.6  | 15.2 | 0.6 | 12.8 | 55.0 | -    | 0.7 | 2.4  |
| 10   | -    | 15.3 | -   | 0.2 | 0.7 | 1.0  | 10.4 | 0.5 | 10.4 | 58.0 | 0.4  | 0.7 | 2.4  |

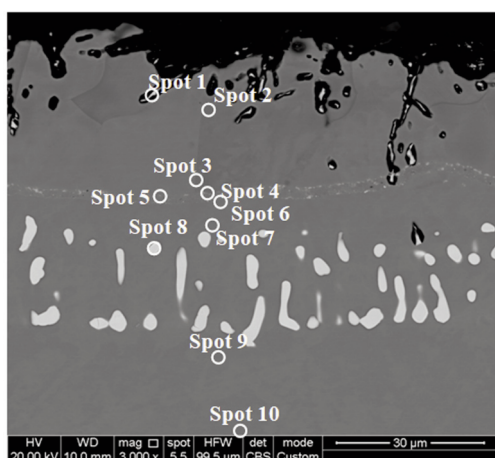


Figure 6. The cross-sectional microstructure of the oxidized Pd+Zr co-doped aluminide coating deposited on the Mar-M247 substrate

diffused from the substrate (Fig.7, Table 1). The XRD pattern (Fig.8) confirmed the presence of the  $\beta$ -NiAl phase, whose lattice parameter increased (0.4%). This proved that palladium dissolved in the  $\beta$ -NiAl phase, enlarged the  $\beta$ -NiAl crystal lattice parameter and the  $\beta$ -(Ni,Pd)Al phase was formed.

The coating consisted of two zones (Fig.9). The outer zone, 20  $\mu$ m thick and the interdiffusion zone, 25  $\mu$ m thick. The outer zone consisted of the  $\beta$ -(Ni,Pd)Al phase, as confirmed by the XRD analysis (Fig.8). The aluminum content decreased from 46.2% close to the surface (Fig. 9, spot 1) to 31.8% close to the boundary between the outer and interdiffusion zones (Fig.9, Table 7 spot 4). The palladium content decreased from 12.2% to 5.5%. Such distribution is typical for diffusive aluminide coatings [30]. Hafnium rich inclusions were observed on the border of two zones (Fig.9, spot 5) and the chain of hafnium rich



inclusions was visible in the outer zone, a few  $\mu\text{m}$  above the border of the zones. The interdiffusion zone contained a large number of precipitates of refractory elements that diffused from the substrate (Fig. 9, spots 6-8). The phenomenon of two zones and a chain of hafnium rich precipitates and inclusions containing refractory elements in the interdiffusion zone was reported by Pytel et al. [30] on the MAR M200 +Hf superalloy.

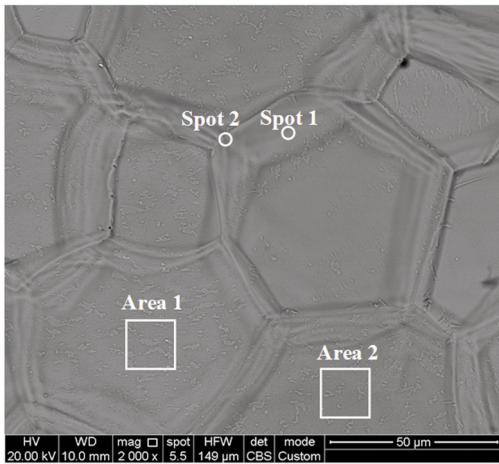
**3.4. Microstructure of the Hf+Pd co-doped coating after oxidation**

Two kinds of areas were clearly visible on the surface of the sample (Fig. 10). The light areas (area1, spot1) were composed of nickel, aluminum, palladium and refractory elements, whereas the dark

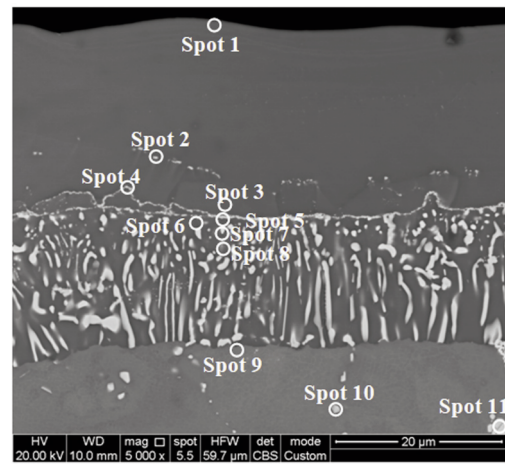
ones (area 2, spot 2,3) were composed of aluminum and oxygen with small amounts of hafnium, palladium and refractory elements. XRD analysis revealed the following phases:  $\alpha\text{-Al}_2\text{O}_3$ ,  $\text{HfO}_2$ ,  $\text{AlNi}_3$ ,  $\text{TiO}_2$  and  $\text{Ni}_{82}\text{Pd}_{18}$  (Fig.11). The dark areas contained oxides, whereas chemical and phase composition of

**Table 6.** Chemical composition on the surface of the the Pd+Hf co-doped aluminide coating deposited on the Mar-M247 substrate, (at.%), Fig.7

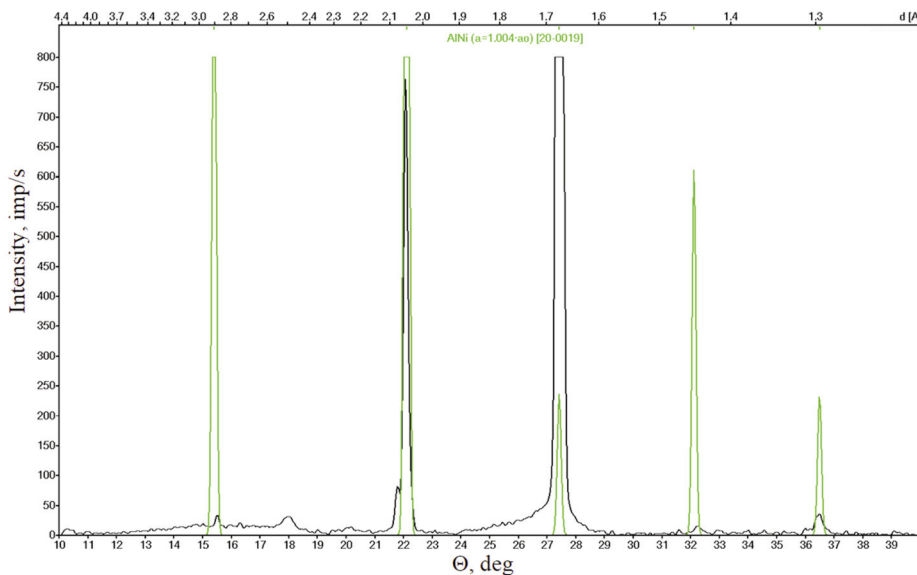
| Area/Spot | Al   | Pd  | Cr  | Fe  | Co  | Ni   |
|-----------|------|-----|-----|-----|-----|------|
| Area 1    | 42.8 | 5.3 | 1.2 | 1.0 | 5.1 | 44.7 |
| Area 2    | 43.9 | 5.8 | 1.1 | 0.8 | 4.8 | 43.6 |
| Spot 1    | 40.5 | 5.7 | 0.9 | 1.0 | 5.1 | 46.7 |
| Spot 2    | 45.4 | 5.6 | 1.0 | 0.8 | 4.7 | 42.9 |



**Figure 7.** Surface morphology (a) and EDS spectrum of area 1 (b) of the the Pd+Hf co-doped aluminide coating deposited on the Mar-M247 substrate



**Figure 9.** The cross-sectional microstructure of the Pd+Hf co-doped aluminide coating deposited on the Mar-M247 substrate

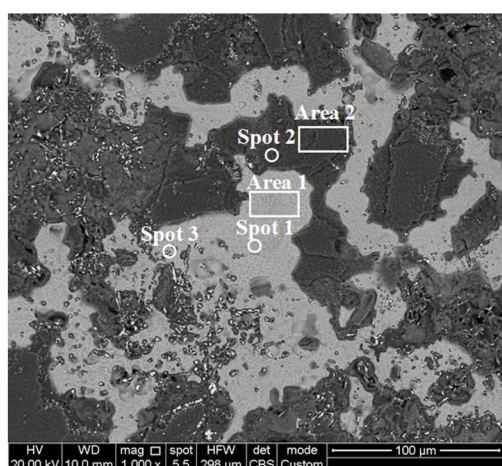


**Figure 8.** XRD diffraction of the Pd+Hf co-doped aluminide coating deposited on the Mar-M247 substrate



**Table 7.** Chemical composition on the cross-section of the palladium hafnium modified aluminide coating deposited on the Mar-M247 substrate (at.%), Fig.9

| Spot | Al   | Mo  | Pd   | Ti   | Cr   | Fe  | Co   | Ni   | Hf   | Ta   | W    |
|------|------|-----|------|------|------|-----|------|------|------|------|------|
| 1    | 46.2 | -   | 12.2 | -    | 1.1  | 1.1 | 5.9  | 52.9 | -    | -    | -    |
| 2    | 35.7 | -   | 6.5  | 4.7  | 2.7  | 1.1 | 4.5  | 34.3 | 5.0  | 4.3  | 1.3  |
| 3    | 38.4 | -   | 4.3  | 0.5  | 3.7  | 1.5 | 6.6  | 44.9 | -    | -    | -    |
| 4    | 31.8 | -   | 5.5  | 6.3  | 3.2  | 1.4 | 4.9  | 34.1 | 6.2  | 5.6  | 1.0  |
| 5    | 26.0 | -   | 4.1  | 0.6  | 4.0  | 1.7 | 5.0  | 32.6 | 13.7 | 4.3  | 1.0  |
| 6    | 37.4 | -   | 4.2  | 2.1  | 8.3  | 0.4 | 6.9  | 44.8 | 0.8  | -    | -    |
| 7    | 19.4 | 3.1 | 3.0  | 0.8  | 13.0 | 2.0 | 10.5 | 28.2 | -    | 1.3  | 17.9 |
| 8    | 31.6 | 0.9 | 3.3  | 0.8  | 8.3  | 1.8 | 8.7  | 36.2 | -    | 1.1  | 7.3  |
| 9    | 16.0 | 0.1 | 0.4  | 1.4  | 8.7  | 1.5 | 10.7 | 56.9 | 0.6  | 0.7  | 3.0  |
| 10   | 7.6  | 1.8 | -    | 0.7  | 16.4 | 0.2 | 11.4 | 43.4 | -    | 0.6  | 17.9 |
| 11   | -    | 0.9 | -    | 35.4 | 2.6  | -   | -    | 9.7  | 4.8  | 34.2 | 12.1 |

**Figure 10.** Surface morphology of the Pd+Hf co-doped aluminide coating deposited on the Mar-M247 substrate

the light areas was the same as the aluminide coating (Figure 7, Table 6). It proves, that after 500 hours of oxidation light areas of the scale composed of  $\alpha$ -Al<sub>2</sub>O<sub>3</sub>, HfO<sub>2</sub>, TiO<sub>2</sub> spalled and the light areas of the coating became clearly visible.

The cross-sectional microstructure of the oxidized coating (Fig. 12) was very similar to the unoxidized

**Table 8.** Chemical composition on the surface of the oxidized Pd+Hf co-doped aluminide coating deposited on the Mar-M247 substrate (at.%), Fig.10

| Area/Spot | O    | Al   | W   | Ta  | Pd  | Ti  | Cr  | Fe  | Co  | Ni   | Hf  |
|-----------|------|------|-----|-----|-----|-----|-----|-----|-----|------|-----|
| Area 1    | -    | 30   | 0.2 | 0.3 | 6.0 | 0.6 | 4.1 | 0.3 | 5.3 | 53.2 | -   |
| Area 2    | 53.3 | 45.8 | -   | -   | -   | -   | 0.4 | -   | -   | 0.4  | 0.1 |
| Spot 1    | -    | 41.4 | 0.9 | 1.2 | 2.1 | 1.2 | 4.8 | 0.4 | 6.8 | 63.2 | -   |
| Spot 2    | 55.1 | 43.2 | -   | -   | 0.2 | -   | 0.5 | -   | 0.1 | 0.5  | -   |
| Spot 3    | 49.5 | 31.1 | -   | 0.8 | -   | 0.1 | 0.8 | -   | 1.0 | 7.4  | 9.9 |

Cross-section of the oxidized coating was similar to the coating before oxidation (Fig. 12)

one (Fig. 9). The same two zones, the chain of Hf rich inclusions on the border of the zones, no oxide scale. The outer zone contained mainly nickel, aluminum and small amounts of palladium and other refractory elements. The interdiffusion zone contained mainly nickel and aluminum with a large number of precipitates of refractory elements. There was no oxide layer.

### 3.5. Oxidation resistance

The oxidation resistance of the Pd+Zr co-doped aluminide coating was compared with the Pd+Hf co-doped one (Fig. 13). Mass changes and samples areas were measured. The accuracy of the measurement was as follows: area - 0.001 cm, weight - 0.0001g. During the initial (incubation) period (40 hours) the weights of both coatings increased. The weight uptakes of the Zr modified coating are bigger (up to 0.5 mg/cm<sup>2</sup>) than of the Hf modified one (up to 0.3 mg/cm<sup>2</sup>). Similar phenomenon was observed by Wei et al. [31]. In the next stage, up to 100 hours, weights of both samples remained stable and then the weight of the hafnium modified one decreased whereas the weight of the other coating remained stable till the end of the experiment.



#### 4. Discussion

Palladium and zirconium co-doped aluminide coatings were successfully deposited on Mar M247 nickel superalloy, see Fig. 1-3 and Tables 2,3. The obtained two-zone structure is typical for aluminide coatings [24, 25]. The thickness ratio of the zones is close to 5:4 and is similar to the results obtained by other authors [32]. Both zones were built of the  $\beta$ -NiAl phase. Palladium concentration is uniform throughout the coating, in both zones (Fig. 3). Palladium dissolved in the  $\beta$ -NiAl phase, enlarged its lattice parameter of 0.6% and the  $\beta$ -(Ni,Pd)Al phase was formed. Palladium substituted Ni atoms in the lattice [8]. Reactive elements did not dissolve in the  $\beta$ -(Ni,Pd)Al phase. Zr and Hf formed inclusions situated at the border of the zones and some Zr rich inclusions were found on the surface of the coating

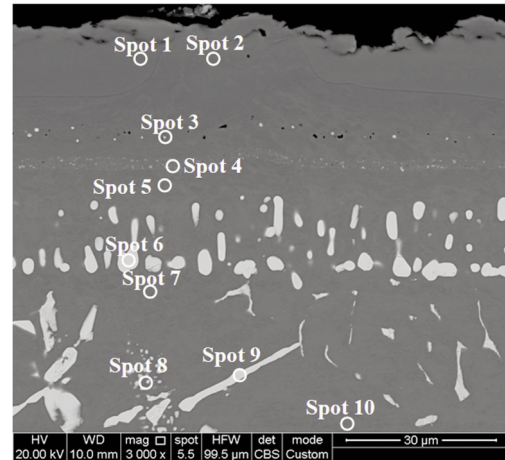


Figure 12. The cross-sectional microstructure of the Pd+Hf co-doped coating after 500 h oxidation

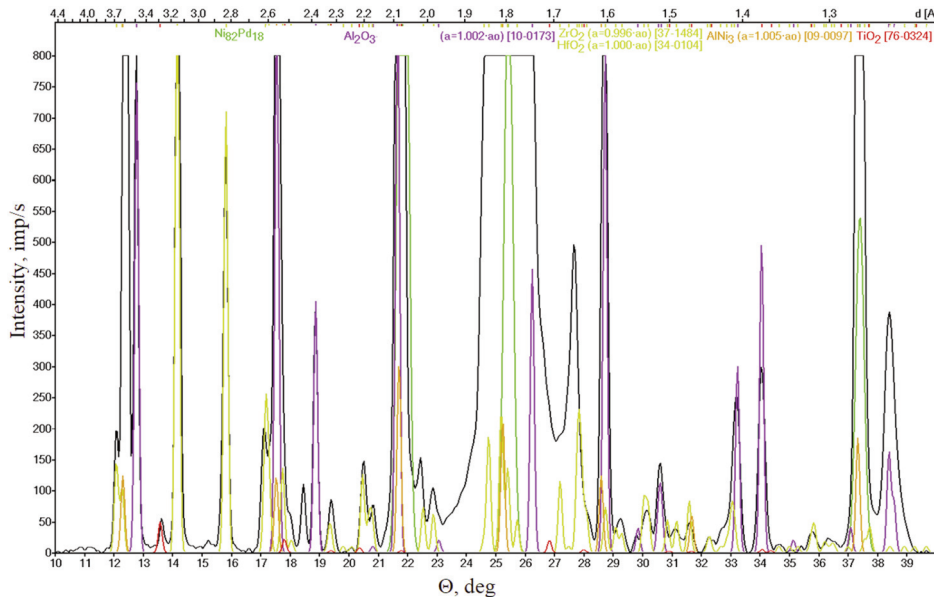
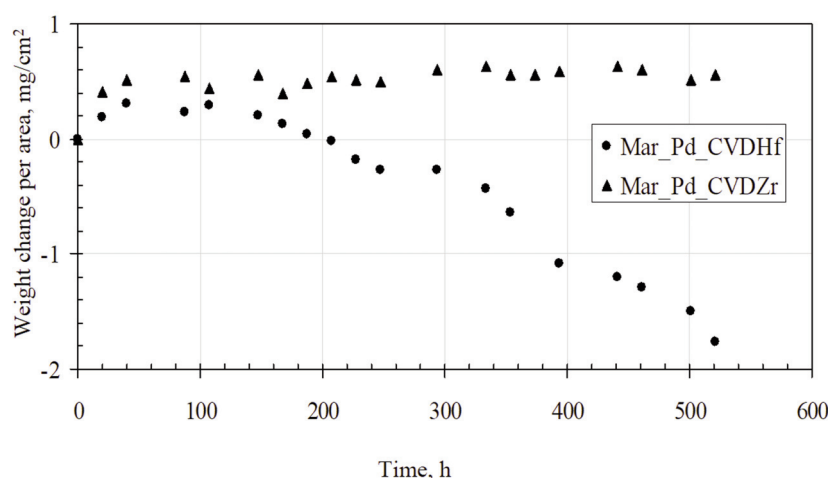


Figure 11. XRD diffraction of the oxidized Pd+Hf co-doped aluminide coating deposited on the Mar-M247 substrate

Table 9. Chemical composition on the cross-section of the oxidized Pd+Hf co-doped aluminide coating deposited on the Mar-M247 substrate (at.%), Fig.12

| Spot | Al   | Mo  | Pd   | Ti   | Cr   | Fe  | Co   | Ni   | Hf  | Ta   | W    |
|------|------|-----|------|------|------|-----|------|------|-----|------|------|
| 1    | 34.5 | -   | 7.6  | 0.4  | 4.0  | 0.4 | 4.6  | 48.1 | -   | -    | -    |
| 2    | 20.5 | -   | 2.0  | 1.3  | 5.1  | 0.4 | 6.9  | 61.3 | -   | 1.1  | 1.5  |
| 3    | 18.7 | -   | 2.0  | 1.2  | 4.6  | 0.3 | 6.5  | 59.0 | 5.2 | 0.8  | 1.7  |
| 4    | 13.6 | -   | 1.6  | 12.8 | 4.3  | 0.4 | 5.9  | 49.6 | 3.4 | 6.5  | 1.9  |
| 5    | 19.1 | -   | 1.6  | 1.3  | 4.4  | 0.3 | 7.3  | 62.7 | -   | 1.2  | 2.0  |
| 6    | -    | 2.6 | -    | 0.4  | 11.0 | 0.5 | 7.4  | 13.8 | -   | 4.9  | 59.4 |
| 7    | 14   | 0.3 | 0.9  | 0.9  | 12   | 0.7 | 11.4 | 56.3 | -   | 0.9  | 2.7  |
| 8    | 3.9  | 0.2 | 30.5 | -    | 2.0  | 0.2 | 2.9  | 19.2 | 5.4 | 32.5 | 3.0  |
| 9    | 3.1  | 2.8 | -    | 1.0  | 21.5 | 0.8 | 12.1 | 24.3 | -   | 2.0  | 32.5 |
| 10   | 11.2 | 0.3 | 0.5  | 0.7  | 14.4 | 0.7 | 12.6 | 55.4 | -   | 0.8  | 3.3  |





**Figure 13.** Oxidation resistance of Pd+Zr and Pd+Hf co-doped aluminide coatings on the Mar-M247 substrate

and in the outer zone. This is evidence that zirconium diffused from the vapor phase through the outer zone and formed inclusions on the border of the zones, whereas hafnium diffused from the substrate through the interdiffusion zone and formed inclusions on the border of the zones (Fig. 3). The similar chain of Zr or Hf rich inclusions was observed at the border of the zones in Zr or Hf modified coatings deposited on CMSX-4 nickel superalloy or pure nickel [25, 26]. During the oxidation process the  $\text{Al}_2\text{O}_3$  scale was formed. The coating below the scale remained intact. Both Zr and Hf diffused through the outer zone and the  $\text{Al}_2\text{O}_3$  layer and formed oxides at the surface. The oxidation resistance of the Pd+Zr co-doped aluminide coating deposited on Mar M247 was compared with the oxidation resistance of the Pd+Hf co-doped coatings deposited on the same Mar M247 nickel superalloy. As indicated by the experimental results, the Zr modified (Ni,Pd)Al coating had significantly better oxidation resistance than the Hf modified one (see Fig.7). It is worth mentioning that Mar M247 nickel superalloy contained 1.5 %wt hafnium. This hafnium diffused from the substrate and formed Hf rich inclusions on the border of the zones (Fig. 3), similarly to hafnium introduced to the coating by the CVD method [25]. Therefore, the analyzed coating should be regarded as the platinum, zirconium and hafnium modified one. After the oxidation, the coating was covered by the  $\text{Al}_2\text{O}_3$  scale. The presence of  $\text{ZrO}_2$  and  $\text{HfO}_2$  phases is an evidence that both Hf and Zr diffused outward to the surface and formed oxides that precipitated at the oxide/scale interface. This phenomenon agrees with the Wu et al. observation [14]. These oxides slowed down Al outward diffusion [15] and changed the oxide scale growth mechanism to the inward oxygen diffusion and reduced the oxide growth rate [16]. This coating had significantly better oxidation resistance than the hafnium modified one (see

Fig.13). It may be assumed that  $\text{ZrO}_2$  inclusions in Pd modified coating improved rumpling resistance similarly to  $\text{ZrO}_2$  inclusions in Pt modified coatings [23].

In the hafnium modified coating hafnium was introduced to the coating in the CVD process and diffused from the substrate. Only a small amount of hafnium (0.1-1wt%) improves the oxidation resistance. Further increase of Hf content causes deterioration of the oxidation resistance [17, 18]. It seems that this phenomenon was observed in this experiment. The oxide layer spalled from the coating (Fig. 10 and 12). The cross-sectional microstructure of the oxidized coating (Fig. 12) was very similar to the unoxidized one (Fig. 9). The same two zones, the chain of Hf rich inclusions on the border of the zones, no oxide scale. When hafnium was introduced to the coating by CVD process only, for example, to the coating deposited on CMSX-4 nickel superalloy, the oxidation resistance was better than for only palladium modified coatings [24], but CMSX-4 superalloy did not contain hafnium [24], unlike Mar-M247. Therefore, it may be assumed that the amount of hafnium introduced to the coating by the CVD method is sufficient to improve its oxidation resistance and the additional hafnium diffusing from the substrate caused the border value of 1% wt to be exceeded [17, 18].

On the other hand, the synergistic effect of palladium, zirconium and hafnium in Pd+Zr co-doped coating was very promising. The oxidation resistance significantly improved. It is worth mentioning that zirconium and hafnium had similar properties and both (a) lowered the growth of the oxide scale, due to the inhibition of aluminum outward diffusion, (b) suppressed formation of interfacial voids because of the strong affinity between RE ions and sulfur, (c) interfacial “pegs”, resulting from higher chemical activity of RE ions contributed to the improvement of

scale adhesion by stronger mechanical bonding at the oxide/metal interface and (d) eliminated the ridge structure and surface rumpling which are the initiators of cracking in the oxide scale [11, 33]. Zr and Hf ions first segregated to the scale/alloy interface and then diffused to the oxide scale surface along oxide grain boundaries. The slow outward diffusion of large Zr and Hf ions stood against the outward diffusion of aluminum ions and the inward diffusion of oxygen. It was called a “blocking effect” and was supposed to be responsible for reducing the alumina scale growth rate [11].

## 5. Conclusions

The microstructure and cyclic oxidation behavior of Pd+Zr and Pd+Hf co-doped coatings deposited on Mar-M247 nickel superalloy were compared. The following conclusions were drawn:

Both coatings consist of two zones, the outer and the interdiffusion zone which are composed of the  $\beta$ -(Ni,Pd)Al phase.

Hafnium and zirconium formed inclusions that precipitated at the border of the zones and close to the surface (only in the Zr+Pd modified coating).

A large number of inclusions containing refractory elements are located in the interdiffusion zone.

Oxidation resistance of the Pd+Zr co-doped aluminide coating was significantly better than the Pd+Hf co-doped one. Hafnium was introduced into the Pd+Hf co-doped coating in two ways (diffusion from the substrate and CVD process) and its content could exceed the border value.

## Acknowledgment

*This research was sponsored by the National Science Centre, Poland (NCN), project number 2015/19/B/ST8/01645*

## Author's contributions

*Conceptualization: J. Romanowska; Methodology: J. Romanowska, Writing, review and editing: J. Romanowska, M. Zagula-Yavorska. Authors read and agreed to the published version of the manuscript.*

## Data Availability Statement

*No additional data.*

## Conflict of Interest

*Authors declared, that they have no conflict of interest to this work.*

## References

- [1] C. Jiang, L. Qian, M. Feng, H. Liu, Z. Bao, M. Chen, S. Zhu, F. Wang, Benefits of Zr addition to oxidation resistance of a single-phase (Ni,Pt)Al coating at 1373K, *Journal of Materials Science and Technology*, 35 (2019) 1334-1344. <https://doi.org/10.1016/j.jmst.2019.03.013>
- [2] M.M. Barjestech, S.M. Abbasi, K. Zangenech-Madar, K. Shirwani, Creep rupture properties of bare and coated polycrystalline nickel-based superalloy Rene 80, *Journal of Mining and Metallurgy, Section B: Metallurgy*, 57(3) (2021) 401-412. <https://doi.org/10.2298/JMMB201203036B>
- [3] M.M. Barjestech, K. Zangenech-Madar, S.M. Abbasi, K. Shirwani, The effect of platinum-aluminide coating features on high temperature fatigue life of nickel-based superalloy Rene 80, *Journal of Mining and Metallurgy, Section B: Metallurgy*, 55(2) (2019) 235-251. <https://doi.org/10.2298/JMMB181214029B>
- [4] B. Pint, I. Wright, Y. Lee, Y. Zhang, K. Průšner, K. Alexander, Substrate and bond coat composition: factors affecting alumina scale adhesion, *Materials Science and Engineering: A*, 245 (1998), 201-211. [https://doi.org/10.1016/S0921-5093\(97\)00851-4](https://doi.org/10.1016/S0921-5093(97)00851-4)
- [5] S. Hong, G. Hwang, W. Han, S. Kang, Cyclic oxidation of Pt/Pd-modified aluminide coating on a nickel-based superalloy at 1150°C, *Intermetallics*, 17 (2009) 381-386. <https://doi.org/10.1016/j.intermet.2008.08.014>
- [6] V. Tolpygo, D. Clarke, Rumpling of CVD (Ni,Pt)Al diffusion coatings under intermediate temperature cycling, *Surface and Coating Technology*, 203 (2009) 3278-3285. <https://doi.org/10.1016/j.surfcoat.2009.04.016>
- [7] S. Alperine, P. Steinmetz, A. Constantini, P. Josso, Structure and high temperature performance of various palladium-modified aluminide coatings: a low cost alternative to platinum aluminides, *Surface and Coating Technology*, 43/44 (1990) 437-360. [https://doi.org/10.1016/0257-8972\(90\)90087-S](https://doi.org/10.1016/0257-8972(90)90087-S)
- [8] S.J. Hong, G.H. Hwang, W.K. Han, S.G. Kang, Cyclic oxidation of Pt/Pd-modified aluminide coating on a nickel-based superalloy at 1150°C, *Intermetallics*, 17 (2009) 381-386. <https://doi.org/10.1016/j.intermet.2008.08.014>
- [9] D. He, H. Guan, X. Sun, X. Jiang, Manufacturing, structure and high temperature corrosion on nickel-base superalloy M38, *Thin Solid Films*, 376 (2000) 144-150. [https://doi.org/10.1016/S0040-6090\(00\)01198-6](https://doi.org/10.1016/S0040-6090(00)01198-6)
- [10] J.A. Nesbitt, B. Nagaraj, J. Williams, Effect of Hf additions to Pt aluminide bond coats on EB-PVD TBC life, *Science Technology*, 4 (2001) 78-92. <https://doi.org/10.1002/9781118787694.ch6>
- [11] D. Li, H. Guo, D. Wang, T. Zhang, S. Gong, X. Hubin, Cyclic oxidation of  $\beta$ -NiAl with various reactive element dopants at 1200°C, *Corrosion Science*, 66 (2013) 125-135. <https://doi.org/10.1016/j.corsci.2012.09.010>
- [12] Y. Wang, J.L. Smialek, M. Suneson, N. Glenn, Oxidation behavior of Hf-modified aluminide coatings on Inconel-718 at 1050°C, *Journal of Coating Science and Technology* (2014) 25-45. <http://doi.org/10.6000/2369-3355.2014.01.01.4>
- [13] R.W. Jackson, D.M. Lipkin, T.M. Pollock, Thermal barrier coatings adherence to Hf modified B2 NiAl bond coatings, *Acta Materialia*, 80 (2014) 39-47.



- <http://doi.org/10.1016/j.actamat.2014.07.033>
- [14] Q. Wu, H.M. Chan, J.M. Rickman, M.P. Hammer, J. Smialek, Effect of Hf<sup>4+</sup> concentration on oxygen grain-boundary diffusion in alumina, *Journal of the American Ceramic Society*, 98 (2015) 3346-3351. <https://doi.org/10.1111/jace.13762>
- [15] B.A. Pint, Experimental observations in support of the dynamic-segregation theory to explain the reactive-element effect, *Oxidation of Metals*, 45 (1996) 1-37. <https://doi.org/10.1007/BF01046818>
- [16] H.B. Guo, D. Wang, H. Peng, S. Gong, H. Xu, Effect of Sm, Gd, Yb, Sc and Nd as reactive elements on oxidation behavior of  $\beta$ -NiAl at 1200°C, *Corrosion Science*, 78 (2014) 369-377. <https://doi.org/10.1016/j.corsci.2013.10.021>
- [17] Y. Wang, M. Suneson, G. Sayre, Synthesis of Hf-modified coatings on Ni-base superalloys, *Surface and Coating Technology*, 15 (2011) 1218-1228. <https://doi.org/10.1016/j.surfcoat.2011.08.031>
- [18] A.W. Cocchardt, Township W. US patent 1961; 3005705
- [19] S. Hamadi, M. Bacos, M. Poulain, A. Seyeux, V. Maurice, P. Marcus, Oxidation resistance of Zr-doped NiAl coating thermochemically deposited on a nickel-based superalloy, *Surface and Coating Technology*, 204 (2009) 756-760. <http://doi.org/10.1016/j.surfcoat.2009.09.073>
- [20] M. Zagula-Yavorska, Microstructure and oxidation performance of undoped and rhodium-doped aluminide coatings on Mar-M247 superalloy, *Archives of Civil and Mechanical Engineering*, 19 (2019) 832-841. <https://doi.org/10.1016/j.acme.2019.04.001>
- [21] H. Mei, Y. Liu, L. Cheng, Comparison of oxidation resistance of NiCoCrAlTaY-coated and uncoated Mar-M247 superalloys in the air at 1150°C, *Journal of Materials Science*, 47 (2012) 2278-2283. <https://doi.org/10.1007/s10853-011-6041-3>
- [22] H. Mei, Y. Liu, L. Cheng, L. Zhang, Corrosion mechanism of a NiCoCrAlTaY coated Mar-M247 superalloy in molten salt vapour, *Corrosion Science*, 55 (2012) 201-204. <https://doi.org/10.1016/j.corsci.2011.10.021>
- [23] L. Qian, X. Fang, K.T. Voisey, V. Nekouie, Z. Zhou, V.V. Silbersmidt, X. Hou, Incorporation and evolution of ZrO<sub>2</sub> nano-particles in Pt-modified aluminide coating for high temperature applications, *Surface and Coating Technology*, 311 (2017) 238-247. <https://doi.org/10.1016/j.surfcoat.2016.12.106>
- [24] M. Zagula-Yavorska, J. Romanowska, M. Pytel, J. Sieniawski, The microstructure and oxidation resistance of the aluminide coatings deposited by the CVD method on pure nickel and hafnium-doped nickel superalloys, *Archives of Civil and Mechanical Engineering*, 15 (4) (2015) 862-872. <https://doi.org/10.1016/j.acme.2015.03.006>
- [25] J. Romanowska, J. Morgiel, Ł. Kolek, P. Kwolek, M. Zagula-Yavorska, Effect of Pd and Hf co-doping of aluminide coatings on pure nickel and CMSX-4 nickel superalloy, *Archives of Civil and Mechanical Engineering*, 18 (2018) 1421-1429. <https://doi.org/10.1016/j.acme.2018.05.007>
- [26] J. Romanowska, E. Dryzek, J. Morgiel, K. Siemek, Ł. Kolek, M. Zagula-Yavorska, Microstructure and positron lifetimes of zirconium modified aluminide coatings, *Archives of Civil and Mechanical Engineering*, 18 (2018) 1150-1155. <https://doi.org/10.1016/j.acme.2018.03.002>
- [27] J. Romanowska, J. Morgiel, M. Zagula-Yavorska, J. Sieniawski, Nanoparticles in hafnium-doped aluminide coatings, *Materials Letters*, 145 (2015) 162-166. <https://doi.org/10.1016/j.matlet.2015.01.089>
- [28] Powder Diffraction File, Release 2002, PDF-2, International Centre for Diffraction Data, Pennsylvania, USA 2002
- [29] K. Kurosaki, D. Araki, Y. Ohishi, H. Muta, K. Konashi, S. Yamanaka, The  $\delta'/\delta$  phase transition in hafnium hydride and deuteride, *Journal of Nuclear Science and Technology*, 52 (2015) 541-545. <http://doi.org/10.1080/00223131.2014.962638>
- [30] M. Pytel, T. Tokarski, M. Góral, R. Filip, Structure of Pd-Zr and Pt-Zr modified aluminide coatings deposited by a CVD method on nickel superalloys, *Kovove Materialy*, 57 (2019) 343-354. [https://doi.org/10.4149/km\\_2019\\_5\\_343](https://doi.org/10.4149/km_2019_5_343)
- [31] L. Wei, H. Peng, F. Jia, L. Zheng, S. Gong, H. Guo, Cyclic oxidation behavior of Hf/Zr co-doped EB-PVD  $\beta$ -NiAl coatings at 1200 °C, *Surface and Coatings Technology*, 276 (2015) 721-725. <https://doi.org/10.1016/j.surfcoat.2015.05.039>
- [32] C. Jiang, S. Li, H. Liu, Z. Bao, J. Zhang, S. Zhu, F. Wang, Effect of Hf addition in (Ni,Pt)Al bond coat on thermal cycling behavior of a thermal barrier coating system at 1100°C, *Corrosion Science*, 166 (2020) 108424. <https://doi.org/10.1016/j.corsci.2019.108424>
- [33] P.Y. Hou, K. Priimak, Interfacial segregation, pore formation, and scale adhesion on NiAl alloys, *Oxidation of Metals*, 63 (2005) 113-130. <https://doi.org/10.1007/s11085-005-1954-3>



## MIKROSTRUKTURA I OTPORNOST NA OKSIDACIJU Pd+Zr I Pd+Hf KO-DOPIRANIH ALUMINIDNIH PREVLAKA NANESENIH NA MAR-M247 SUPERLEGURU NIKLA

J. Romanowska \*, M. Zagula-Yavorska

Politehnički univerzitet Rzešov, Odeljenje za nauku o materijalima, Fakultet za mašinstvo i aeronautiku,  
Rzešov, Poljska

### Apstrakt

*Pd+Zr i Pd+Hf ko-dopirane aluminidne prevlake nanesene su na superleguru nikla Mar-M247 galvanizacijom paladijuma praćenom cirkonizacijom ili hafnizacijom. Obe prevlake su se sastojale od dve zone, spoljne i interdifuzione zone koja se sastoji od  $\beta$ -(Ni,Pd)Al faze. Hafnijum i cirkonijum su formirali inkluzije deponovane na ivici zona i blizu površine (samo u Zr+Pd modifikovanoj prevlaci). Otpornost na oksidaciju aluminidne prevlake ko-dopirane sa Pd+Zr bila je značajno bolja od one ko-dopirane sa Pd+Hf. Sadržaj hafnijuma u Pd+Hf ko-dopiranoj prevlaci mogao bi premašiti granicu.*

**Ključne reči:** Superlegure nikla; Aluminidne prevlake; Hafnijum; Cirkonijum; Oksidacija

